Adaptive control for UAVs equipped with a robotic arm

Nishant Awdeshkumar Pandey(119247556)[a], Tyler Barrett(113469879)[a], Rishikesh Jadhav(119256534).[a]

[a]University of Maryland, College Park

November 2022

Abstract

The problem of trajectory tracking control for a quadrotor aerial vehicle equipped with a robotic manipulator is addressed in this exercise (aerial manipulator). The controller is divided into two layers: the top layer contains an inverse kinematics algorithm that computes the motion references for the actuated variables, and the bottom layer contains a motion control algorithm that tracks the upper layer's motion references. A model-based control scheme is used for this purpose, with modelling uncertainties compensated by an adaptive term. The proposed scheme's stability is demonstrated using Lyapunov arguments. Finally, simulations are run to demonstrate results.

Keywords: aerial manipulation; adaptive control; model-based control; Lyapunov arguments; inverse kinematics algorithm; motion control algorithm

1 Introduction

The problem of motion control of the end-effector of a robot manipulator mounted on a quadrotor helicopter is addressed in this exercise using a hierarchical control architecture. Position and attitude dynamics are not decoupled in UAVs without arms due to the presence of the arm. As a result, an adaptive solution is proposed to deal with this aspect. In the top layer, an inverse kinematics algorithm computes the motion references for the actuated variables, such as the vehicle's position and yaw angle, as well as the manipulator's joint variables.An adaptive model-based motion control algorithm is in charge of tracking the motion references in the bottom layer: a vehicle position controller computes the thrust force and the reference values for pitch and roll angles; then, an attitude controller computes the moments acting on the quadrotor based on the pitch-roll references, while the manipulator controller computes the joint torques. It is worth noting that the model used to design the proposed control law excludes some inertial coupling terms; this choice allows the design of the quadrotor position and attitude controllers to be decoupled. As a result, the adaptive term not only allows for dealing with unavoidable modeling uncertainties, but also for mitigating the effect of dynamical terms that were purposefully left out of the control law's design. Furthermore, a thorough stability analysis of the system is performed using Lyapunov arguments.

2 Literature Review

Over the last years, Unmanned Aerial Vehicles (UAVs) have witnessed a scientific community interest, due to the developments in sensors and communication that make UAVs more suitable for a large number of applications, such as surveillance and remote monitoring, cooperative transportation, rescue missions and monitoring of hostile environments. Among UAVs, there is a great interest for Vertical Takeoff and Landing (VTOL) vehicles, such as multi-rotor helicopters. Motion control of multi-rotors is a widely investigated but still challenging issue, since they are under-actuated systems and, often, are equipped with limited sensing devices. Conventional approaches to UAV control have been based on linear controller design and robust H_∞ controllers, requiring model linearization about a set of equilibrium conditions. Linear controllers are characterized by satisfactory performance near the design conditions or in hovering, but performance degradation is usually observed when the aircraft moves away from these conditions. To overcome these drawbacks, many nonlinear controllers have been proposed, including model predictive control, back stepping and sliding mode techniques. Recently, adaptive control laws have been proposed, e.g., in [Palunko, I., Fierro, R], where a feedback linearization approach is adopted and the mathematical model of the UAV is written in such a way to point out its linear dependency on the position of the center of gravity. In [Antonelli, G., Cataldi, E., Arrichiello, F., Giordano, P.R., Chiaverini, S., Franchi, A.], the effect of constant exogenous forces and moments, and the presence of unknown dynamic parameters (e.g., the position of the center of mass) have been considered. Since it is possible to make a conceptual separation between position and orientation of a quadrotor, hierarchical controllers, based on an inner-outer loop, have been successfully proposed as, e.g., in [Kendoul, F., Fantoni,

I., Lozano, R.]. A relatively recent application field is aerial manipulation by means of UAVs equipped with grippers or robotic arms. This is a challenging issue since the vehicle is characterized by unstable dynamics and the presence of the gripper/arm, as well as the held object, can cause nontrivial coupling effects. Different mechanical structures have been added to the aerial vehicle: in [Pounds, P., Bersak, D., Dollar, A.] a compliant gripper, composed of four fingers, is proposed, while in [Mellinger,D.,Lindsey,Q.,Shomin,M.,Kumar,V] several light-weight low-complexity grippers are tested. More recently, in order to extend their manipulation capabilities, research platforms including multi-DOFs manipulators mounted on VTOL UAVs have been developed (aerial manipulators, see [Ruggiero, F., Lippiello, V., Ollero, A.] for a brief literature review). The manipulator's motion generates reaction forces on the UAV that can have destabilizing effects. The problem of interaction between the arm and the vehicle has been tackled in [Huber, F., Kondak, K., Krieger, K., Sommer, D., Schwarzbach, M., Laiacker, M., Kossyk, I., Parusel, S., Haddadin, S., Albu-Schaffer, A.] and [Kondak, K., Huber, F., Schwarzbach, M., Laiacker, M., Sommer, D., Bejar, M., Ollero, A.], where the dynamic coupling of an helicopter with a 7-DOFs robotic manipulator is analyzed, while in [Antonelli, G., Cataldi, E.] an adaptive scheme, aimed at compensating the manipulator's mass and the interaction caused by its movements, is proposed. In [Fumagalli, M., Naldi, R., Macchelli, A., Forte, F., Keemink, A., Stramigioli, S., Carloni, R., Marconi, L.], the authors present the design, modeling and control of an aerial manipulator consisting of a quadrotor helicopter endowed with a robotic manipulator based on a 3-DOFs delta structure and a 3-DOFs end-effector. In [Kim, S., Choi, S., Kim, H.], an adaptive controller for a quadrotor equipped with a 2-DOFs manipulator is designed and experimentally validated. In [Orsag, M., Korpela, C., Oh, P.], a model reference adaptive control is proposed for a light-weight prototype 3-arm manipulator, each arm with 2 DOFs. In [Lippiello, V., Ruggiero, F.] and [Ryll, M., Muscio, G., Pierri, F., Cataldi, E., Antonelli, G., Caccavale, F., Franchi, A.], a Cartesian impedance control is developed to counteract the effects of contact forces and external disturbances. Hierarchical control of aerial manipulators to perform tasks in operational space has been introduced in [Arleo, G., Caccavale, F., Muscio, G., Pierri, F.], where a model-based control approach is pursued, and in [Kannan, S., Bezzaoucha, S., Guzman, S.Q., Dentler, J., Olivares-Mendez, M.A., Voos, H.], where model-free motion control laws are adopted. The algorithm in [Arleo, G., Caccavale, F., Muscio, G., Pierri, F] has been extended via an adaptive term for compensating the model uncertainties.

3 Modeling

Let us consider a system composed by a quadrotor vehicle equipped with a n-DOF robotic arm, depicted in figure. 1.

3.1 Kinematics

In this section the aim is to find the enf effector velocity(both angular and linear).

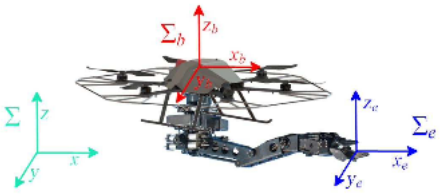

Figure 1: Quadrotor and robotic arm system with the corresponding frames.

Symbol description is as follows:

Σ:World fixed inertial reference frame

Σ_b:Vehicle body-fixed reference frame with origin at the vehicle center of mass

Σ_e:Frame attached to the end effector.

$\mathbf{p}_b$:(3 x 1) vector that gives vehicle's position with respect to the world fixed inertial reference frame

$\mathbf{R}_b$:While its orientation is given by the rotation matrix

If yaw-pitch-roll (ZYX) angles are ψ, θ, ϕ respectively then:

$$\mathbf{R}_b(\phi_b) = \begin{bmatrix} C_\psi C_\theta & C_\psi S_\theta S_\phi - S_\psi C_\phi & C_\psi S_\theta S_\phi + S_\psi C_\phi \\ S_\psi C_\theta & S_\psi S_\theta S_\phi + C_\psi C_\phi & C_\psi S_\theta S_\phi - C_\psi C_\phi \\ -S_\theta & C_\theta S_\phi & C_\theta C_\phi \end{bmatrix}, \quad (1)$$

where $\phi_b = \begin{bmatrix} \psi & \theta & \phi \end{bmatrix}^T$ is the triple of ZYX yaw-pitch-roll angles and C_γ and S_γ denote, respectively, $\cos\gamma$ and $\sin\gamma$. The rotation matrix($\mathbf{R}_b$) is obtained by multiplication of three (3x3) matrices which give rotation of vehicle about Z,Y,X axis respectively. Position and orientation of the end effector frame with respect to the world frame are:

$$\mathbf{p}_e = \mathbf{p}_b + \mathbf{R}_b \mathbf{p}^b_{eb}, \quad (2)$$

$$\mathbf{R}_e = \mathbf{R}_b \mathbf{R}^b_e, \quad (3)$$

where the vector $\mathbf{p}^b_{eb}$ and the matrix $\mathbf{R}^b_e$ describe the position and the orientation of $\sum_e$ with respect to $\sum_b$, respectively.
By differentiating (2) and (3) linear and angular velocities are obtained as follows:

$$\frac{d\boldsymbol{p}_e}{dt} = \frac{d\boldsymbol{p}_b}{dt} - \boldsymbol{S}(\boldsymbol{R}_b \boldsymbol{p}^b_{eb})\boldsymbol{\omega}_b + \mathbf{R}_b \frac{d\boldsymbol{p}^b_{eb}}{dt}, \quad (4)$$

$$\boldsymbol{\omega}_e = \boldsymbol{\omega}_b + \mathbf{R}_b \boldsymbol{\omega}^b_{eb}, \quad (5)$$

$\boldsymbol{S}(\cdot)$: (3x3) skew-symmetric matrix operator performing the cross product (Siciliano et al., 2009),

$\boldsymbol{\omega}^b_{eb} = \boldsymbol{R}^T_b(\boldsymbol{\omega}_e - \boldsymbol{\omega}_b)$:Relative angular velocity between the end effector and the frame $\sum_b$, expressed in $\sum_b$.

Let $\mathbf{q}$ be the (n × 1) vector of joint coordinates of the manipulator. The (6 x 1) generalized velocity with respect to $\sum_b$,$\boldsymbol{v}_{eb}^b$=$\begin{bmatrix}\frac{d\boldsymbol{p}_{eb}^{bT}}{dt} & \boldsymbol{\omega}_{eb}^{bT}\end{bmatrix}^T$ can be obtained using manipulator Jacobian $\mathbf{J}_{eb}^b$.

If $\mathbf{p}_{eb}^b(\boldsymbol{q})$ and $\mathbf{R}_e^b(\boldsymbol{q})$ represent the usual direct kinematics equations of a ground-fixed manipulator with respect to its base frame, $\sum_b$ then,

$$\boldsymbol{v}_{eb}^b = \boldsymbol{J}_{eb}^b(\boldsymbol{q})\frac{d\boldsymbol{q}}{dt} \tag{6}$$

To obtain the generalized end effector velocity, $\boldsymbol{v}_e = [\frac{d\boldsymbol{p}_e^T}{dt} \quad \boldsymbol{\omega}_e^T]^T$ along with the equations (4), (5), (6) the following parameters are needed:

$$\boldsymbol{T}_A(\phi_b) = \begin{bmatrix}\boldsymbol{I}_3 & \boldsymbol{O}_3 \\ \boldsymbol{O}_3 & \boldsymbol{T}(\phi_b)\end{bmatrix}, \boldsymbol{T}(\phi_b) = \begin{bmatrix}0 & -S_\psi & C_\psi C_\theta \\ 0 & -C_\psi & S_\psi C_\theta \\ 1 & 0 & -S_\theta\end{bmatrix},$$

$$\boldsymbol{J}_b = \begin{bmatrix}\boldsymbol{I}_3 & -\boldsymbol{S}(\boldsymbol{R}_b\boldsymbol{p}_{eb}^b) \\ \boldsymbol{O}_3 & \boldsymbol{I}_3\end{bmatrix}, \boldsymbol{J}_{eb} = \begin{bmatrix}\boldsymbol{R}_b & \boldsymbol{O}_3 \\ \boldsymbol{O}_3 & \boldsymbol{R}_b\end{bmatrix}\boldsymbol{J}_{eb}^b,$$

where $\boldsymbol{I}_m$ and $\boldsymbol{O}_m$ denote (m × m) identity and null matrices, respectively.
Using the equations above:

$$\boldsymbol{v}_e = \boldsymbol{J}_b(\boldsymbol{q},\phi_b)\boldsymbol{T}_A(\phi_b)\frac{d\boldsymbol{x}}{dt} + \boldsymbol{J}_{eb}(\boldsymbol{q},\boldsymbol{R}_b)\frac{d\boldsymbol{q}}{dt} \tag{7}$$

Where $\boldsymbol{x}_b = \begin{bmatrix}\boldsymbol{p}_b^T & \phi_b^T\end{bmatrix}^T$
Since the quadrotor is an under-actuated system, with 4 independent control inputs available against the 6 DOFs, the position and the yaw angle are usually the controlled variables, while pitch and roll angles are used as intermediate control inputs for position control. Hence, it is worth rewriting the vector $\boldsymbol{x}_b$ as follows:

$$\boldsymbol{x}_b = \begin{bmatrix}\boldsymbol{\eta}_b^T & \sigma_b^T\end{bmatrix}^T, \boldsymbol{\eta}_b = \begin{bmatrix}\boldsymbol{p}_b^T & \psi\end{bmatrix}^T, \boldsymbol{\sigma_b} = [\theta \quad \psi]^T$$

If the vector of controlled variables is $\boldsymbol{\zeta} = \begin{bmatrix}\boldsymbol{\eta}_b^T & \boldsymbol{q}^T\end{bmatrix}$
Then, the differential kinematics (7) becomes

$$\begin{aligned}\boldsymbol{v}_e &= \boldsymbol{J}_\eta(\boldsymbol{q},\phi_b)\frac{d\boldsymbol{\eta}_b}{dt} + \boldsymbol{J}_\sigma(\boldsymbol{q},\phi_b)\frac{d\boldsymbol{\sigma}_b}{dt} + \boldsymbol{J}_{eb}(\boldsymbol{q},\boldsymbol{R}_b)\frac{d\boldsymbol{q}}{dt} \\ &= \boldsymbol{J}_\zeta(\boldsymbol{\sigma}_b,\zeta)\frac{d\boldsymbol{\zeta}}{dt} + \boldsymbol{J}_\sigma(\boldsymbol{\sigma}_b,\zeta)\frac{d\boldsymbol{\sigma}_b}{dt}\end{aligned} \tag{8}$$

where $\boldsymbol{J}_\eta$ is is composed by the first 4 columns of $\boldsymbol{J}_b\boldsymbol{T}_A(\phi_b)$,$\boldsymbol{J}_\sigma$ by the last 2 columns of $\boldsymbol{J}_b\boldsymbol{T}_A(\phi_b)$ and $\boldsymbol{J}_\zeta = [\boldsymbol{J}_\eta \quad \boldsymbol{J}_{eb}]$.

3.2 Dynamics

The dynamic model can be derived (these results are derived in Lippiello and Ruggiero (2012)) by considering the so-called Euler-Lagrange formulation, in which the mechanical structure can be characterized by the function L=K+U where K and U denote the total kinetic and potential energies of the system, respectively The Lagrange equations are then expressed by:

$$\frac{d}{dt}\frac{\partial L}{\partial \dot{\xi}_i} - \frac{\partial L}{\partial \xi_i} = u_i,$$

where i=1,...,n_ξ,ξ_i is the i-th generalized coordinate of $\boldsymbol{\xi}$, and u_i is the associated i-th generalized force.
The total kinetic energy is given by the sum of the contributions relative to the motion of the aerial vehicle and the motion of each link of the manipulator. The Vehicle kinetic energy contribution is given by:

$$K_b = \frac{1}{2}m_b\dot{\boldsymbol{p}}_p^T\dot{\boldsymbol{p}}_b + \frac{1}{2}\boldsymbol{\omega}_b^T\boldsymbol{R}_b\boldsymbol{H}_b\boldsymbol{R}_b^T\boldsymbol{\omega}_b, \tag{9}$$

where m_b and $\boldsymbol{H}_b$ are the mass and the inertia matrix of the vehicle. $\boldsymbol{H}_b$ is constant as it is with respect to $\sum_b$. We know that $\boldsymbol{\omega}_b$=$\boldsymbol{R}_b^T\boldsymbol{T}_b\dot{\phi}_b = \boldsymbol{Q}\dot{\phi}_b$,

$$K_b = \frac{1}{2}m_b\dot{\boldsymbol{p}}_p^T\dot{\boldsymbol{p}}_b + \frac{1}{2}\boldsymbol{Q}^T\dot{\phi}_b^T\boldsymbol{H}_b\boldsymbol{Q}\dot{\phi}_b, \tag{10}$$

On the other hand, the kinetic energy contribution of each link of the robotic manipulator is given by

$$K_{l_i} = \frac{1}{2}m_{l_i}\dot{\boldsymbol{p}}_{l_i}^T\dot{\boldsymbol{p}}_{l_i} + \frac{1}{2}\boldsymbol{\omega}_{l_i}^T\boldsymbol{R}_b\boldsymbol{R}_{l_i}^b\boldsymbol{H}_{l_i}\boldsymbol{R}_b^{l_i}\boldsymbol{R}_b^T\boldsymbol{\omega}_{l_i}, \tag{11}$$

where $\boldsymbol{R}_{l_i}^b$, is the rotation matrix between the frame associated to the center of mass of the i-th link and $\sum_b$,while m_{l_i} and $\boldsymbol{H}_{l_i}$ are the mass and the constant inertia matrix of the same link i, respectively. By taking into account the above equations (9), (10), (11) the total kinetic energy can be expressed as

$$K = \frac{1}{2}\dot{\boldsymbol{\xi}}^T\boldsymbol{M}\dot{\boldsymbol{\xi}},$$

where $\boldsymbol{M}$ is an $(n_\xi \times n_\xi)$ symmetric and positive definite inertia matrix, whose block-elements are:

$$\boldsymbol{M}_{11} = \big(m_b + \sum_{i=1}^n m_{l_i}\big)\boldsymbol{I}_3$$

$$\boldsymbol{M}_{22} = \boldsymbol{Q}^T\boldsymbol{H}_b\boldsymbol{Q}$$

$$+m_{l_i} + \sum_{i=1}^n \big(m_{l_i}\boldsymbol{T}_b^T\boldsymbol{S}(\boldsymbol{R}_b\boldsymbol{p}_{bl_i}^b)^T\boldsymbol{S}(\boldsymbol{R}_b\boldsymbol{p}_{bl_i})\boldsymbol{T}_b + \boldsymbol{Q}^T\boldsymbol{R}_{l_i}^b\boldsymbol{H}_{l_i}\boldsymbol{R}_b^{l_i}\boldsymbol{Q}\big)$$

$$\boldsymbol{M}_{33} = \sum_{(i=1)}^n \big(m_{l_i}\boldsymbol{J}_p^{(l_i)^T}\boldsymbol{J}_p^{(l_i)} + \boldsymbol{J}_O^{(l_i)^T}\boldsymbol{R}_{l_i}^b\boldsymbol{H}_{l_i}\boldsymbol{R}_b^{l_i}\boldsymbol{J}_O^{(l_i)}\big)$$

$$\boldsymbol{M}_{12} = \boldsymbol{M}_{21}^T = -\sum_{i=1}^n \big(m_{l_i}\boldsymbol{S}(\boldsymbol{R}_b\boldsymbol{p}_{bl_i}^b)\boldsymbol{T}_b\big)$$

$$\boldsymbol{M}_{13} = \boldsymbol{M}_{31}^T = \sum_{i=1}^n \big(m_{l_i}\boldsymbol{R}_b\boldsymbol{J}_p^{(l_i)}\big)$$

$$\boldsymbol{M}_{23} = \boldsymbol{M}_{32}^T = \sum_{i=1}^n \big(\boldsymbol{Q}^T\boldsymbol{R}_{l_i}^b\boldsymbol{H}_{l_i}\boldsymbol{R}_b^{l_i}\boldsymbol{J}_O^{(l_i)}$$

$$-m_{l_i}\big(m_{l_i}\boldsymbol{T}_b^T\boldsymbol{S}(\boldsymbol{R}_b\boldsymbol{p}_{bl_i}^b)^T\boldsymbol{R}_b\boldsymbol{J}_p^{(l_i)}\big)$$

in which $\boldsymbol{I}_\alpha$ denotes the $(\alpha \times \alpha)$ identity matrix.
$\boldsymbol{p}_{l_i}$: the position of the center of mass of the link i with respect to $\sum_i$, the following relationship holds

$$\boldsymbol{p}_{l_i} = \boldsymbol{p}_b + \boldsymbol{R}_b\boldsymbol{p}_{bl_i}^b,$$

where $\boldsymbol{p}_{bl_i}^b$ denotes the vector position of the center of mass of the link i with respect to $\sum_b$. Moreover, Siciliano et al.(2009) consider the following expressions:

$$\dot{\boldsymbol{p}}_{bl_i}^b = \boldsymbol{J}_{P_1}^{l_i}\dot{q}_1 + \cdots + \boldsymbol{J}_{P_i}^{l_i}\dot{q}_i = \boldsymbol{J}_P^{(l_i)}\dot{q}$$

$$\boldsymbol{\omega}_{l_i}^b = \boldsymbol{J}_{O_1}^{l_i}\dot{q}_1 + \cdots + \boldsymbol{J}_{O_i}^{l_i}\dot{q}_i = \boldsymbol{J}_O^{(l_i)}\dot{q}$$

where $\omega_{l_i}^b$ is the angular velocity of the i-th manipulator frame with respect to $\sum_b$, and where $\boldsymbol{J}_P^{(l_i)}$ and $\boldsymbol{J}_O^{(l_i)}$ are the contributions of the Jacobian columns relative to the joint velocities up to the current link i. Where,

$$\dot{\boldsymbol{p}}_{l_i} = \dot{\boldsymbol{p}}_b - \boldsymbol{S}(\boldsymbol{R}_b\boldsymbol{p}_{bl_i}^b)^T\boldsymbol{R}_b\boldsymbol{J}_P^{(l_i)}\dot{\boldsymbol{q}},$$

Similarly, the total potential energy of the system can be computed by adding the potential energy of the

vehicle(U_b) with the potential energy of the link(U_{l_i}) which gives:

$$U = m_b g e_3^T \boldsymbol{p}_b + g \sum_{i=1}^{n} \left[m_l, e_3^T \left(\boldsymbol{p}_b \boldsymbol{R}_b \boldsymbol{p}_{bl_i}^b \right) \right]$$

where $g = 9.8 m/s^2$, e_3 is a (3×1) vector selecting the axes of $\sum_i$ where the gravity acts. After analysing and applying Euler-Lagrange formulation the above equations the dynamic model can be stated in the following manner:

$$\boldsymbol{M}(\boldsymbol{\xi})\ddot{\boldsymbol{\xi}} + \boldsymbol{C}(\boldsymbol{\xi}, \dot{\boldsymbol{\xi}})\dot{\boldsymbol{\xi}} + \boldsymbol{g}(\boldsymbol{\xi}) + \boldsymbol{d}(\boldsymbol{\xi}, \dot{\boldsymbol{\xi}}) = \boldsymbol{u}, \quad (12)$$

where $\xi = \begin{bmatrix} \boldsymbol{x}_b^T & \boldsymbol{q}^T \end{bmatrix}^T \in \mathbb{R}^{(6+n\times 1)}$,
$\boldsymbol{M}$: Symmetric and positive definite inertia matrix of the system,
$\boldsymbol{C}$: Matrix of Coriolis and centrifugal terms,
$\boldsymbol{g}$: Vector of gravity forces,
$\boldsymbol{d}$: Disturbances, such as aerodynamic effects, and modeling uncertainties,
$\boldsymbol{u}$: Vector of inputs,

$$\boldsymbol{u} = \begin{bmatrix} \boldsymbol{u}_f \\ \boldsymbol{u}_\mu \\ \boldsymbol{u}_\tau \end{bmatrix} = \begin{bmatrix} \boldsymbol{R}(\phi_b)\boldsymbol{f}_b^b \\ \boldsymbol{T}^T(\phi_b)\boldsymbol{R}(\phi_b)\boldsymbol{\mu}_b^b \\ \boldsymbol{\tau} \end{bmatrix}, \quad (13)$$

where $\boldsymbol{\tau}$ is the (n × 1) vector of the manipulator joint torques, while $\boldsymbol{f}_b^b = \begin{bmatrix} 0 & 0 & f_z \end{bmatrix}^T$ and $\boldsymbol{\mu}_b^b = \begin{bmatrix} \mu_\psi & \mu_\theta & \mu_\phi \end{bmatrix}^T$ are, respectively, the forces and the torques generated by the 4 motors of the quadrotor, expressed in the frame $\sum_b$.Both f_z and μ_b^b are related to the four actuation forces output by the quadrotor motors $\boldsymbol{f}$ via (Nonami et al., 2010).

$$\begin{bmatrix} f_z \\ \boldsymbol{\mu}_b^b \end{bmatrix} = \begin{bmatrix} 1 & 1 & 1 & 1 \\ 0 & l & 0 & -l \\ -l & 0 & -l & 0 \\ c & -c & c & -c \end{bmatrix} \begin{bmatrix} f_1 \\ f_2 \\ f_3 \\ f_4 \end{bmatrix} = \boldsymbol{\Gamma}\boldsymbol{f}, \quad (14)$$

where l > 0 is the distance from each motor to the vehicle center of mass, c = γ_d/γ_t,and γ_d, γ_t are the drag and thrust coefficient, respectively. The detailed analysis of the equation (12) gives the matrices for $\boldsymbol{M}(\boldsymbol{\xi}), \boldsymbol{C}(\boldsymbol{\xi}, \dot{\boldsymbol{\xi}}), \boldsymbol{g}(\boldsymbol{\xi})$. The inertia matrix can be viewed as a block matrix:

$$\boldsymbol{M}(\xi) = \begin{bmatrix} \boldsymbol{M}_{11} & \boldsymbol{M}_{12} & \boldsymbol{M}_{13} \\ \boldsymbol{M}_{12}^T & \boldsymbol{M}_{22} & \boldsymbol{M}_{23} \\ \boldsymbol{M}_{13}^T & \boldsymbol{M}_{23}^T & \boldsymbol{M}_{33} \end{bmatrix},$$

Where $\boldsymbol{M}_{11} \in \mathbb{R}^{3\times 3}, \boldsymbol{M}_{22} \in \mathbb{R}^{3\times 3}, \boldsymbol{M}_{33} \in \mathbb{R}^{n\times n}, \boldsymbol{M}_{12} \in \mathbb{R}^{3\times 3}, \boldsymbol{M}_{13} \in \mathbb{R}^{3\times n}, \boldsymbol{M}_{23} \in \mathbb{R}^{3\times n}$. Similarly, matrix

$$\boldsymbol{C}(\boldsymbol{\xi}, \dot{\boldsymbol{\xi}}) = \begin{bmatrix} \boldsymbol{C}_1 \\ \boldsymbol{C}_2 \\ \boldsymbol{C}_3 \end{bmatrix}, \boldsymbol{g}(\boldsymbol{\xi}) = \begin{bmatrix} \boldsymbol{g}_1 \\ \boldsymbol{g}_2 \\ \boldsymbol{g}_3 \end{bmatrix},$$

where $\boldsymbol{C}_1 \in \mathbb{R}^{3\times(6+n)}, \boldsymbol{C}_2 \in \mathbb{R}^{3\times(6+n)}, \boldsymbol{C}_3 \in \mathbb{R}^{n\times(6+n)}$ and $\boldsymbol{g}_1 \in \mathbb{R}^3, \boldsymbol{g}_2 \in \mathbb{R}^3, \boldsymbol{g}_3 \in \mathbb{R}^n$

4 Kinematic Control Scheme

A two-layer control scheme is proposed: on the top layer, an inverse kinematics algorithm computes the motion references for the quadrotor-controlled variables and the arm joints based on the desired end-effector trajectory; on the bottom layer, motion control is designed to track the reference trajectories output by the top layer. (Figure. 2).

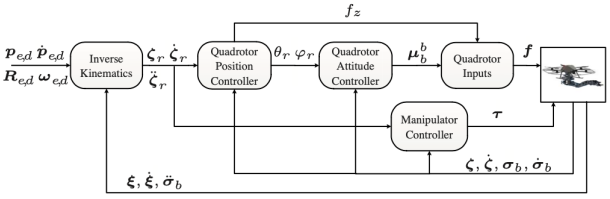

Figure 2: Block scheme of the control architecture

In the following, it is assumed that
$\dim\{\boldsymbol{\zeta}\} = n + 4 \geq \dim\{\boldsymbol{v}_e\} = 6$, .i.e, the number of DOFs characterizing the vehicle-manipulator system is, at least, equal to the dimension of the assigned task.

4.1 Inverse Kinematics

The time derivative of the differential kinematics (8),

$$\dot{\boldsymbol{v}}_e = \dot{\boldsymbol{J}}_\zeta(\boldsymbol{\sigma}_b, \zeta)\dot{\zeta} + \boldsymbol{J}_\zeta(\boldsymbol{\sigma}_b, \zeta)\ddot{\boldsymbol{\zeta}} + \dot{\boldsymbol{J}}_{\boldsymbol{\sigma}}(\boldsymbol{\sigma}_b, \zeta)\dot{\boldsymbol{\sigma}}_b + \dot{\boldsymbol{J}}_{\boldsymbol{\sigma}}(\boldsymbol{\sigma}_b, \zeta)\ddot{\boldsymbol{\sigma}}_b, \quad (15)$$

is considered to derive a second order closed-loop inverse kinematics algorithm (Caccavale et al., 1997), in charge of computing the trajectory references for the motion control loops at the bottom layer

$$\ddot{\zeta}_r = \boldsymbol{J}_\zeta^\dagger(\boldsymbol{\sigma}_b, \boldsymbol{\zeta})(\dot{\boldsymbol{v}}_{e,d} + \boldsymbol{K}_v(\boldsymbol{v}_{e,d} - \boldsymbol{v}_e) + \boldsymbol{K}_p\boldsymbol{e})$$

$$-\boldsymbol{J}_\zeta^\dagger(\boldsymbol{\sigma}_b, \boldsymbol{\zeta})\left(\dot{\boldsymbol{J}}_\zeta(\boldsymbol{\sigma}_b, \dot{\boldsymbol{\zeta}}) + \boldsymbol{J}_\sigma(\boldsymbol{\sigma}_b, \boldsymbol{\zeta})\ddot{\boldsymbol{\sigma}}_b + \dot{\boldsymbol{J}}_\sigma(\boldsymbol{\sigma}_b, \boldsymbol{\zeta})\dot{\boldsymbol{\sigma}}_b\right), \quad (16)$$

where $\boldsymbol{J}_\zeta^\dagger = \boldsymbol{J}_\zeta^T(\boldsymbol{J}_\zeta\boldsymbol{J}_\zeta^T)^{-1}$ is a right pseudoinverse of $\boldsymbol{J}_\zeta$, $\boldsymbol{K}_v$ and $\boldsymbol{K}_p$ are symmetric positive definite gain matrices, given by:

$\boldsymbol{K}_p = \begin{bmatrix} \boldsymbol{K}_{(p,P)} \\ \boldsymbol{K}_{(p,O)} \end{bmatrix}$, $\boldsymbol{K}_v = \begin{bmatrix} \boldsymbol{K}_{(v,P)} \\ \boldsymbol{K}_{(v,O)} \end{bmatrix} = \boldsymbol{K}_p = \begin{bmatrix} \boldsymbol{K}_{(v,P)} \\ \boldsymbol{K}_{(v,O)}\boldsymbol{I}_3, \end{bmatrix}$

with $k_{(v,O)}$ a positive constant. $\boldsymbol{e}$ is the kinematic inversion error between the desired end-effector pose $\boldsymbol{x}_{e,d}$ and the actual pose $\boldsymbol{x}_e$ computed via the direct kinematics on the basis of $\boldsymbol{\zeta}$ and $\boldsymbol{\sigma}_b$ in the following manner:
end-effector position error: $\boldsymbol{e}_p = \boldsymbol{p}_d - \boldsymbol{p}(\boldsymbol{q})$
The above equation gives the displacement between the desired and the current end-effector trajectory.
end-effector orientation error: $\boldsymbol{e}_{O,Eul} = \boldsymbol{\omega}_d - \boldsymbol{\omega}(\boldsymbol{q})$
The above equation showcases the difference between the desired and current orientation quantities. The above equations gives the unit quaternions which are used for error can be computation as (Chiaverini and Siciliano, 1999).

$$\boldsymbol{e} = \begin{bmatrix} \boldsymbol{e}_P \\ \boldsymbol{e}_O \end{bmatrix} = \begin{bmatrix} \boldsymbol{P}_{e,d} - \boldsymbol{P}_e(\boldsymbol{\sigma}_b, \zeta) \\ \boldsymbol{R}_{e,d}\tilde{\boldsymbol{\epsilon}}(\boldsymbol{\sigma}_b, \zeta) \end{bmatrix}, \quad (17)$$

where $\tilde{\boldsymbol{\epsilon}}$ is the vectorial part of the unit quaternion extracted from the mutual orientation matrix $\boldsymbol{R}_{e,d}^T\boldsymbol{R}_e(\boldsymbol{\sigma}_b, \boldsymbol{\zeta})$. If n + 4 > 6 the system is kinematically redundant and the redundant DOFs can be exploited to fulfill secondary tasks, otherwise, if no secondary tasks are required, the internal motions, i.e, motions of the structure that do not change the end-effector pose, must be stabilized via a suitable designed damping term to be

projected onto the null space of $\boldsymbol{J}_\zeta$ (Hsu et al., 1988),i.e.,

$$\ddot{\zeta}_r = \boldsymbol{J}_\zeta^\dagger\big(\boldsymbol{\sigma}_b,\boldsymbol{\zeta}\big)(\dot{\boldsymbol{v}}_{e,d} + \boldsymbol{K}_v(\boldsymbol{v}_{e,d} - \boldsymbol{v}_e) + \boldsymbol{K}_p\boldsymbol{e}\big)$$
$$-\boldsymbol{J}_\zeta^\dagger(\boldsymbol{\sigma}_b,\boldsymbol{\zeta})\big(\dot{\boldsymbol{J}}_\zeta(\boldsymbol{\sigma}_b,\dot{\boldsymbol{\zeta}}) + \boldsymbol{J}_\sigma(\boldsymbol{\sigma}_b,\boldsymbol{\zeta})\ddot{\boldsymbol{\sigma}}_b + \dot{\boldsymbol{J}}_\sigma(\boldsymbol{\sigma}_b,\boldsymbol{\zeta})\dot{\boldsymbol{\sigma}}_b\big)$$
$$-\boldsymbol{N}(\boldsymbol{J}_\zeta)(k_N\boldsymbol{I}_{N+4} + \dot{\boldsymbol{N}})\dot{\boldsymbol{\zeta}},$$

where $\boldsymbol{N}(\boldsymbol{J}_\zeta)$ is a projector onto the null space of the Jacobian $\boldsymbol{J}_\zeta$; is a possible choice is $\boldsymbol{N}(\boldsymbol{J}_\zeta) = \boldsymbol{I}_{n+4} - \boldsymbol{J}_\zeta^\dagger\boldsymbol{J}_\zeta$.

4.2 Motion Control

Once ζ_r and its derivatives are computed by (16), they are fed to the motion control to achieve the desired motion. The proposed controller is an extension of that in Arleo et al. (2013), in turn, it is a hierarchical inner-outer loop control scheme: the outer loop is designed to track the vehicle reference position; then, by using the relation between the force vector $\boldsymbol{u}_f$ and the quadrotor attitude, a reference value for the roll and pitch angles is devised and fed to the attitude controller (inner loop). Finally, a controller for the arm joint positions is designed. In order to globally linearize the closed-loop dynamics, the following adaptive control law can be considered.In order to design the control law, it is worth rewriting the system model(12):

$$\overline{\boldsymbol{M}}(\boldsymbol{\xi})\ddot{\boldsymbol{\xi}} + \boldsymbol{C}(\boldsymbol{\xi},\dot{\boldsymbol{\xi}})\dot{\boldsymbol{\xi}} + \boldsymbol{g}(\boldsymbol{\xi}) + \boldsymbol{d}(\boldsymbol{\xi},\dot{\boldsymbol{\xi}}) + \Delta\boldsymbol{M}(\boldsymbol{\xi})\ddot{\boldsymbol{\xi}} = \boldsymbol{u}, \quad (18)$$

where the matrix $\overline{\boldsymbol{M}}$ is obtained by setting to zero the second and third columns of $\boldsymbol{M}_{12}$:

$$\overline{\boldsymbol{M}}(\xi) = \begin{bmatrix} \boldsymbol{M}_{11} & \overline{\boldsymbol{M}}_{12} & \boldsymbol{M}_{13} \\ \boldsymbol{M}_{12}^T & \boldsymbol{M}_{22} & \boldsymbol{M}_{23} \\ \boldsymbol{M}_{13}^T & \boldsymbol{M}_{23}^T & \boldsymbol{M}_{33} \end{bmatrix},$$

with $\overline{\boldsymbol{M}}_{12} = \begin{bmatrix}\boldsymbol{m}_{12} & \boldsymbol{0}_3 & \boldsymbol{0}_3\end{bmatrix}$, where $\boldsymbol{m}_{12}$ denotes the first coloumn $\boldsymbol{M}_{12}$, and $\boldsymbol{0}_3$ is the (3×1) null vector. In order to globally linearize the closed-loop dynamics, the following adaptive control law can be considered:

$$\boldsymbol{u} = \boldsymbol{M}(\boldsymbol{\xi})\boldsymbol{\alpha} + \boldsymbol{C}(\boldsymbol{\xi},\dot{\boldsymbol{\xi}})\dot{\boldsymbol{\xi}} + \boldsymbol{g}(\boldsymbol{\xi}) + \widehat{\boldsymbol{d}}(\boldsymbol{\xi},\dot{\boldsymbol{\xi}}), \quad (19)$$

where the auxiliary input $\boldsymbol{\alpha}$ can be partitioned according to (13) as $\boldsymbol{\alpha} = [\boldsymbol{\alpha}_1^T\ \boldsymbol{\alpha}_2^T\ \boldsymbol{\alpha}_3^T]^T$ with $\boldsymbol{\alpha}_\phi = [\alpha_\psi\ \alpha_\phi\ \alpha_\varphi]^T$. The term $\widehat{\boldsymbol{d}} = [\widehat{\boldsymbol{d}}_1^T\ \widehat{\boldsymbol{d}}_2^T\ \widehat{\boldsymbol{d}}_3^T]$ is an estimate of the disturbance $\boldsymbol{d}$ in (18). The auxiliary controls $\boldsymbol{\alpha}_3$ and $\boldsymbol{\alpha}_1$ and α_ψ can be chosen as:

$$\boldsymbol{\alpha}_3 = \ddot{\boldsymbol{q}}_r + \boldsymbol{K}_{q,V}(\dot{\boldsymbol{q}}_r - \dot{\boldsymbol{q}}) + \boldsymbol{K}_{q,P}(\boldsymbol{q}_r - \boldsymbol{q}),$$
$$\boldsymbol{\alpha}_1 = \ddot{\boldsymbol{p}}_r + \boldsymbol{K}_{p,V}(\dot{\boldsymbol{p}}_r - \dot{\boldsymbol{p}}) + \boldsymbol{K}_{p,P}(\boldsymbol{p}_r - \boldsymbol{p}),$$
$$\alpha_\psi = \ddot{\psi} + k_{\psi,V}(\dot{\psi}_r - \dot{\psi}) + K_{\psi,P}(\psi_r - \psi),$$

where $\boldsymbol{K}_{*,V}, \boldsymbol{K}_{*,P} (* = \{q,p\})$ are symmetric positive definite matrices and $k_{\psi,V}, k_{\psi,P}$ are positive scalar gains.

Quadrotor position controller

On the basis of (19), the following expression of $\boldsymbol{u}_f$

$$\boldsymbol{u}_f = \boldsymbol{M}_{11}\boldsymbol{\alpha}_1 + \boldsymbol{m}_{12}\alpha_\psi + \boldsymbol{M}_{13}\boldsymbol{\alpha}_3 + \boldsymbol{C}_1\dot{\boldsymbol{\xi}} + \boldsymbol{g}_1 + \widehat{\boldsymbol{d}}_1, \quad (20)$$

where the function dependencies have been dropped for notation compactness It can be noted that, since the manipulator links are much lighter than the vehicle body, the elements of matrix $\boldsymbol{M}_{12}$ are often negligible with respect to those of $\boldsymbol{M}_{11}$ (Arleo et al., 2013). Therefore, in practice, $\boldsymbol{u}_f$ in (20) is very close to the ideal control input. In view of (11), u_f depends on the attitude of the quadrotor via the relation

$$\boldsymbol{u}_f = \boldsymbol{h}(\boldsymbol{f}_z,\boldsymbol{\sigma}_b) \Longrightarrow \begin{bmatrix} u_{f,x} \\ u_{f,y} \\ u_{f,z} \end{bmatrix} = \begin{bmatrix} (c_\psi s_\theta c_\varphi + s_\psi s_\varphi) f_z \\ (s_\psi s_\theta c_\varphi - c_\psi s_\varphi) f_z \\ c_\theta c_\varphi f_z \end{bmatrix} \quad (21)$$

Therefore, the total thrust, f_z, and reference trajectories for the roll and pitch angles to be fed to the inner loop can be computed as

$$f_z = ||\boldsymbol{u}_f||, \quad (22)$$
$$\theta_r = arctan\Big(\frac{u_{f,x}c_\psi + u_{f,y}s_\psi}{u_{f,z}}\Big), \quad (23)$$
$$\phi_r = arcsin\Big(\frac{u_{f,x}s_\psi - u_{f,y}c_\psi}{||u_f||}\Big), \quad (24)$$

Remark 1. It is worth noticing that (23)–(24) are not well defined if $||u_f||$ vanishes, but from (22) it can happen only if $f_z = 0$, namely in presence of total thrust null. Moreover, they imply that both θ_r and ϕ_r are defined in $(-\pi/2, \pi/2)$: this is a reasonable assumption for quadrotor vehicles.

Quadrotor attitude controller

Once the reference value for roll and pitch angles have been computed, the control inputs α_θ and α_φ can be obtained via

$$\alpha_\theta = \ddot{\theta}_r + K_{\theta,V}(\dot{\theta}_r - \dot{\theta}) + K_{\theta,P}(\theta_r - \theta), \quad (25)$$
$$\alpha_\varphi = \ddot{\varphi}_r + K_{\varphi,V}(\dot{\varphi}_r - \dot{\varphi}) + K_{\varphi,P}(\varphi_r - \varphi) \quad (26)$$

where $k_{\theta,V}, k_{\theta,P}, k_{\varphi,V}, k_{\varphi,P}$ positive scalar gains. It is worth noticing that (25) and (26) require the knowledge of the time derivative of θ_r and φ_r, that can not be directly obtained by (21), but only via numerical differentiation. Since in a practical scenario θ_r and φ_r are likely to be affected by noise, it can be realistic compute the reference velocities ($\dot{\theta_r}$ and $\dot{\varphi_r}$) by using suitable filters but their derivative can be very noisy, thus it is possible to modify (25) and (26) by adopting simple PD control laws as

$$\overline{\alpha}_\theta = k_{\theta,V}(\dot{\theta}_r - \dot{\theta}) + k_{\theta,P}(\theta_r - \theta),$$
$$\overline{\alpha}_\varphi = k_{\varphi,V}(\dot{\varphi}_r - \dot{\varphi}) + k_{\varphi,P}(\varphi_r - \varphi).$$

Finally, $\boldsymbol{u}_\mu$ can be computed as

$$\boldsymbol{u}_\mu = \boldsymbol{M}_{12}^T\boldsymbol{\alpha}_1 + \boldsymbol{M}_{22}\boldsymbol{\alpha}_2 + \boldsymbol{M}_{23}\boldsymbol{\alpha}_3 + \boldsymbol{C}_2\dot{\boldsymbol{\xi}} + \boldsymbol{g}_2 + \widehat{\boldsymbol{d}}_2,$$

and, from (13), the vehicle torques as

$$\boldsymbol{\mu}_b^b = \boldsymbol{R}_b^T(\phi_b)\boldsymbol{T}^{-T}(\phi_b)\boldsymbol{u}_\mu.$$

Computation of quadrotor inputs. Once f_z and $\boldsymbol{\mu}_b^b$ have been computed, the four actuation forces of the vehicle rotors can be easily obtained by inverting the (14) ,i.e.,

$$\boldsymbol{f} = \boldsymbol{\Gamma}^{-1}\begin{bmatrix} \boldsymbol{f}_z \\ \boldsymbol{\mu}_b^b \end{bmatrix}$$

Manipulator control . Finally, the torques acting on the manipulator joints can be computed as

$$\boldsymbol{u}_\mu = \boldsymbol{M}_{12}^T\boldsymbol{\alpha}_1 + \boldsymbol{M}_{23}^T\boldsymbol{\alpha}_2 + \boldsymbol{M}_{33}\boldsymbol{\alpha}_3 + \boldsymbol{C}_3\dot{\boldsymbol{\xi}} + \boldsymbol{g}_3 + \widehat{\boldsymbol{d}}_3$$

4.3 Uncertainties estimation

By considering the control law (20),
If the input $\overline{\boldsymbol{\alpha}}_2 = [\alpha_\psi \ \overline{\alpha}_\phi \ \overline{\alpha}_\varphi]^T$ in lieu of $\boldsymbol{\alpha}_2$, also

$$\Delta \boldsymbol{M}(\boldsymbol{\xi}) = \boldsymbol{M}(\boldsymbol{\xi}) - \overline{\boldsymbol{M}}(\boldsymbol{\xi}),$$

and

$$\Delta \boldsymbol{\alpha} = \boldsymbol{\alpha} - \overline{\boldsymbol{\alpha}},$$
$$\overline{\alpha} = [\boldsymbol{\alpha}_1^T \overline{\boldsymbol{\alpha}}_2^T \boldsymbol{\alpha}_3^T]^T,$$

then the closed-loop dynamics is:

$$\ddot{\boldsymbol{\xi}} = \boldsymbol{\alpha} - \Delta\boldsymbol{\alpha} - \boldsymbol{M}(\boldsymbol{\xi})^{-1}(\Delta \boldsymbol{M}\overline{\boldsymbol{\alpha}} + \boldsymbol{d} - \widehat{\boldsymbol{d}}), \ (27).$$

Thus, the compensation term $\widehat{\boldsymbol{d}}$ has to take into account not only the modeling uncertainties, $\boldsymbol{d}$, but also the perturbation given by the practical implementation of the control law, namely the use of $\overline{\boldsymbol{M}}$ and $\overline{\boldsymbol{\alpha}}$ instead of $\boldsymbol{M}$ and $\boldsymbol{\alpha}$ in (19). To this aim, let us rearrange the (27) as

$$\ddot{\boldsymbol{\xi}} = \boldsymbol{\alpha} - \boldsymbol{\delta} + \widehat{\boldsymbol{\delta}} = \boldsymbol{\alpha} - \widetilde{\boldsymbol{\delta}}, (28),$$

where

$$\boldsymbol{\delta} = \Delta\boldsymbol{\alpha} + \boldsymbol{M}(\boldsymbol{\xi})^{-1}(\Delta \boldsymbol{M}\overline{\boldsymbol{\alpha}} + \boldsymbol{d}) \ , \ \widehat{\boldsymbol{\delta}} = \boldsymbol{M}(\boldsymbol{\xi})^{-1}\widehat{\boldsymbol{d}}.$$

A good approximations of the term $\boldsymbol{\delta}$ can be obtained by resorting to a parametric model, i.e.,

$$\boldsymbol{\delta} = \boldsymbol{\Lambda}(\boldsymbol{\xi})\boldsymbol{\chi} + \boldsymbol{\varsigma}$$

where $\boldsymbol{\Lambda}$ is a $(n + 6 \times p)$ regressor matrix, $\boldsymbol{\chi}$ is a vector of constant parameters and $\boldsymbol{\varsigma}$ is the interpolation error. Of course, not all uncertainties can be rigorously characterized by a linear-in-the-parameters structure, however, this modeling assumption is not too restrictive, since it has been demonstrated that it is valid for a wide class of functions (Caccavale et al., 2013). The elements of the regressor matrix can be chosen as Radial Basis Functions (RBFs)

$$\lambda_{i,h}(\boldsymbol{\xi}) = exp\Big(-\frac{||\boldsymbol{\xi} - \boldsymbol{c}_{i,h}||}{2\sigma^2}\Big)$$

where $c_{i,h}$ and σ are the centroids and the width of the function, respectively. According to the Universal Interpolation Theorem any continuous function can be approximated (in the $\mathscr{L}_p$-norm sense, $p \in [1, \infty)$) (Haykin, 1999), by a RBF-newtork with suitably chosen centroids and a common width, provided that the basis functions $\lambda_{i,h}(\boldsymbol{\xi}, \dot{\boldsymbol{\xi}})$ are continuous, bounded, integrable and with non-null integral over $\boldsymbol{R}^{3n}$. Since $\boldsymbol{\delta}$ can be reasonably assumed continuous and the RBFs satisfy the conditions of the theorem, there exists a RBF-network , i.e., a suitable sets of weights, widths and centroids, capable of approximating $\boldsymbol{\delta}$ to any degree of accuracy. Thus, the interpolation error $\boldsymbol{\varsigma}$ in can be reasonably assumed norm bounded,

$$||\boldsymbol{\varsigma}(t) \leq \bar{\varsigma}||, \ \forall t \geq 0$$

An estimate,

$$\hat{\boldsymbol{\delta}} = \boldsymbol{\Lambda}(\boldsymbol{\xi}, \dot{\boldsymbol{\xi}})\hat{\boldsymbol{\chi}}, (29)$$

of $\boldsymbol{\delta}$ can be obtained by integrating the following update law for the unknown parameters $\boldsymbol{\chi}$:

$$\dot{\hat{\boldsymbol{\chi}}} = \frac{1}{\beta}\boldsymbol{\Lambda}^{\boldsymbol{T}}\boldsymbol{B}^{\boldsymbol{T}}\boldsymbol{Q}\begin{bmatrix}\widetilde{\boldsymbol{\xi}} \\ \dot{\widetilde{\boldsymbol{\xi}}}\end{bmatrix}, (30)$$

where β is a positive scalar gain, $\boldsymbol{Q}$ is a symmetric and positive definite matrix, $\boldsymbol{B} = [\boldsymbol{O}_{\boldsymbol{6+n}} \ \boldsymbol{I}_{\boldsymbol{6+n}}]$ and $\widetilde{\boldsymbol{\xi}} = \boldsymbol{\xi}_{\boldsymbol{r}} - \boldsymbol{\xi}$ is the inner loop error. Then, $\widehat{\boldsymbol{d}}$ can be easily obtained as $\widehat{\boldsymbol{d}} = \boldsymbol{M}(\boldsymbol{\xi})\widehat{\boldsymbol{\delta}}$.

Stability Analysis

Inner Loop
By considering (27), the following dynamics for the inner loop error $\widetilde{\xi}$ can be derived

$$\dddot{\widetilde{\boldsymbol{\xi}}} = -\boldsymbol{\Omega}_V\ddot{\widetilde{\boldsymbol{\xi}}} - \boldsymbol{\Omega}_P\dot{\widetilde{\boldsymbol{\xi}}} + \dot{\widetilde{\boldsymbol{\delta}}}, (31)$$

where ($*$ = V, P)

$$\boldsymbol{\Omega}_* = \begin{bmatrix} -\boldsymbol{K}_{1,*} & O_3 & O_3 \\ O_3 & -\boldsymbol{K}_{2,*} & O_3 \\ O_3 & O_3 & -\boldsymbol{K}_{3,*} \end{bmatrix}, (32)$$

with $\boldsymbol{K}_{2,*} = diag\{K_{\psi,*}, K_{\theta,*}, K_{\varphi,*}\}$. Let us rearrange (31) in the state space form, by considering $\widetilde{\boldsymbol{z}} = [\widetilde{z}_1^T \ \widetilde{z}_2^T]^T = [\widetilde{\boldsymbol{\xi}}^T \ \dot{\widetilde{\boldsymbol{\xi}}}^T]^T$ and assuming $\boldsymbol{\varsigma} = \boldsymbol{0}$,(30) as

$$\dot{\widetilde{\boldsymbol{z}}} = \boldsymbol{\Omega}\widetilde{\boldsymbol{z}} + \boldsymbol{B}\dot{\widetilde{\boldsymbol{\delta}}} = \boldsymbol{\Omega}\widetilde{\boldsymbol{z}} + \boldsymbol{B}\boldsymbol{\Lambda}\dot{\widetilde{\boldsymbol{\chi}}}, (33)$$

where $\widetilde{\boldsymbol{\chi}} = \boldsymbol{\chi} - \hat{\boldsymbol{\chi}}$ and $\boldsymbol{\Omega} = \begin{bmatrix} \boldsymbol{O}_{6+n} & \boldsymbol{I}_{6+n} \\ -\boldsymbol{\Omega}_V & -\boldsymbol{\Omega}_P \end{bmatrix}$, The following theorem can be stated for the inner loop error convergence.

Theorem 1. Given the system and the update law (30), for any set of positive definite matrix gains $\boldsymbol{K}_{1,*}, \boldsymbol{K}_{2,*}$ and $\boldsymbol{K}_{3,*} (* = V, P)$, the equilibrium $\widetilde{\boldsymbol{z}} = \boldsymbol{0}$ is globally asymptotically stable, while the parameters error $\widetilde{\boldsymbol{\chi}}$.

Proof In order to analyze the stability of the system (33), the following Lyapunov candidate function could be considered

$$\boldsymbol{V}_i = \frac{\boldsymbol{1}}{\boldsymbol{2}}\boldsymbol{z}^{\ T}\boldsymbol{Q}\boldsymbol{z} + \frac{\beta}{2}\widetilde{\boldsymbol{\chi}}^T\widetilde{\boldsymbol{\chi}}.$$

The time derivative of V_i yields

$$V_i = -\boldsymbol{z}^T\boldsymbol{P}_z\boldsymbol{z} + \boldsymbol{z}^T\boldsymbol{Q}\boldsymbol{B}\boldsymbol{\Lambda}\widetilde{\boldsymbol{\chi}} + \beta\dot{\widetilde{\boldsymbol{\chi}}}^T\widetilde{\boldsymbol{\chi}}.$$

where $\boldsymbol{P}_z = -(\boldsymbol{Q}\boldsymbol{\Omega} + \boldsymbol{\Omega}^T\boldsymbol{Q})$ is the symmetric and positive definite solution of the Lyapunov equation that always exists since $\boldsymbol{\Omega}$ is Hurwitz. By assuming the parameter $\boldsymbol{\chi}$ constant or, at least, slowly-varying, and by considering the update law (30), V_i can be rewritten as

$$\dot{\boldsymbol{V}}_i = -\boldsymbol{z}^T\boldsymbol{P}_z\boldsymbol{z} + \boldsymbol{z}^T\boldsymbol{Q}\boldsymbol{B}\boldsymbol{\Lambda}\dot{\widehat{\boldsymbol{\chi}}} + \beta\dot{\widetilde{\boldsymbol{\chi}}}^T\widetilde{\boldsymbol{\chi}} = -\boldsymbol{z}^T\boldsymbol{P}_z\boldsymbol{z}$$

Since $\boldsymbol{P}_z$ is positive definite, $\dot{\boldsymbol{V}}_i$ is negative semidefinite; this guarantees the boundedness of $\boldsymbol{z}$ and $\widetilde{\boldsymbol{\chi}}$. By invoking the Barbalat's lemma (Khalil, 1996), it can be recognized that $\dot{V}_i \to 0$, which implies the global asymptotic convergence to $\boldsymbol{0}$ of $\boldsymbol{z}$ as t $\to\infty$, while, as usual in direct adaptive control (Astrom and Wittenmark, 1995), $\widetilde{\boldsymbol{\chi}}$ is only guaranteed to be uniformly bounded, i.e., $||\widetilde{\boldsymbol{\chi}}|| \leq \overline{\chi}$.

Corollary 1 In the presence of the persistency of excitation (PE) condition i.e, if there exist positive scalars k_1, k_2, T such that:

$$k_1\boldsymbol{I}_p \geq \int_t^{t+T} \Lambda^T(\xi(\sigma), \dot{\xi}(\sigma))\Lambda(\xi(\sigma), \dot{\xi}(\sigma))d\sigma \geq k_2\boldsymbol{I}_p,$$

both $\widetilde{\boldsymbol{z}}$ and $\widetilde{\boldsymbol{\chi}}$ are exponentially convergent to zero.

Kinematic control outer loop

Under the assumption of perfect acceleration tracking (i.e.$\ddot{\boldsymbol{\zeta}} = \ddot{\boldsymbol{\zeta}}_r$), by substituting (14) in (13), the following holds

$$\dot{\boldsymbol{v}}_{e,d} - \dot{\boldsymbol{v}}_e = -\boldsymbol{K}_v(v_{e,d} - \boldsymbol{v}_e) - \boldsymbol{K}_p \boldsymbol{e}, \quad (34)$$

Let us consider, the following inverse kinematics error

$$\epsilon = \begin{bmatrix} \epsilon_P \\ \epsilon_O \end{bmatrix}, \epsilon_P = \begin{bmatrix} e_P \\ \dot{e_P} \end{bmatrix}, \epsilon_O = \begin{bmatrix} e_O \\ \widetilde{\omega}_e \end{bmatrix},$$

where e_P and e_O are defined in (15), while $\widetilde{\omega}_e = \omega_{e,d} - \omega_e$.

Theorem 2 Given the system (34), there exists a set of positive definite matrix gains $\boldsymbol{K}_p$ and $\boldsymbol{K}_v$ chosen as in the kinematic control scheme with $k_{v,O} > \frac{1}{2}$, such that the equilibrium $\epsilon = 0$ is exponentially stable.

Proof To prove the asymptotic stability of the equilibrium point $\epsilon = 0$ let us consider the following candidate Lyapunov function (Chiaverini and Siciliano, 1999)

$$V_o = (\eta_d - \eta)^2 + (\epsilon_d - \epsilon)^T(\epsilon_d - \epsilon) + \widetilde{\omega}_e^T \widetilde{\omega}_e + \epsilon_P^T \boldsymbol{Q}_P \epsilon_P$$

where $\eta(\eta_d)$ and $\epsilon(\epsilon_d)$ are the scalar part and the vector part of the unit quaternion representing the end-effector (desired) orientation and $\boldsymbol{Q}_P$ is a symmetric and positive matrix. The time derivative of V_o is given by

$$\dot{V}_o = -\boldsymbol{e}_O^T \boldsymbol{K}_{p,O} \boldsymbol{e}_O - 2\widetilde{\omega}_e^T K_{v,O} \widetilde{\omega} - 2\widetilde{\omega}_e^T K_{p,O} e_O$$

$$+\epsilon_P^T (\boldsymbol{Q}_P A_P + A_P^T \boldsymbol{Q}_P) \epsilon_P, \quad (35)$$

where $K_{*,O}(* = v, p)$ is the matrix including the last three row of matrix $K_{*,}$ and

$$A_P = \begin{bmatrix} O_3 & I_3 \\ -K_{p,P} & -K_{v,P} \end{bmatrix}.$$

with $K_{*,P}(* = v, p)$ the matrix including the first three row of matrix K_*. Since $\boldsymbol{A}_P$ is Hurwitz, always exists a matrix $\boldsymbol{P}_P$, symmetric and positive definite, solution of the Lyapunov equation in (35), hence

$$\dot{V}_o \leq -\lambda_m(K_{p,O}) ||e_O||^2 - 2\lambda_m(K_{v,O}) ||\widetilde{\omega}_e||^2$$

$$-2\lambda_M(K_{p,O}) ||\widetilde{\omega}_e|| ||e_O|| - \lambda_m(P_{p,}) ||e_p||^2$$

$$\leq -\begin{bmatrix} ||e_O|| \\ ||\widetilde{\omega}_e|| \end{bmatrix}^T \Xi \begin{bmatrix} ||e_O|| \\ ||\widetilde{\omega}_e|| \end{bmatrix} - \lambda_m(P_{p,}) ||e_p||^2$$

with

$$\Xi = \begin{bmatrix} \lambda_m(K_{p,O}) & -\lambda_M(K_{p,O}) \\ -\lambda_M(K_{p,O}) & 2\lambda_m(K_{v,O}) \end{bmatrix},$$

and $\lambda_m(\cdot)$ and $\lambda_M(\cdot)$ representing the minimum and maximum eigenvalue of a matrix. If the following holds

$$\lambda_m(K_{v,o}) > \frac{\lambda_M^2(K_{p,o})}{2\lambda_m(K_{p,o})},$$

matrix Ξ is positive definite, therefore $\dot{V}_o$ can be upper bounded as

$$\dot{V}_o \leq -\lambda_m(\Xi) ||\epsilon_O||^2 - \lambda_m(\Xi) ||\epsilon_P||^2 \leq -\lambda_\epsilon ||\epsilon||^2$$

where $\lambda_\epsilon = min\{\lambda_m(\Xi), \lambda_m(\Xi)\}$.
Thus, since $\dot{V}_o$ is negative definite the error ϵ is asymptotically convergent to zero.

Two-loops dynamics

For the two-loops dynamics, by considering the following Lyapunov candidate function

$$V = V_o(\epsilon) + V_i(z),$$

it is straightforward derived that $\dot{V}$ is negative definite and both ϵ and $\boldsymbol{z}$ are globally asymptotically convergent to zero. Moreover the convergence is exponential in the absence of interpolation error ($\boldsymbol{\varsigma} = 0$) and in the presence of PE for the regressor $\boldsymbol{\Lambda}$.

Theorem 3 Under the assumption of perfect acceleration tracking, in the presence of the PE condition and in the absence of the interpolation error($\boldsymbol{\varsigma} = 0$) , on the basis of Corollary 1 and Theorem 2, ϵ, $\hat{\boldsymbol{\zeta}}$ and $\widehat{\boldsymbol{\chi}}$ are exponentially convergent to zero.

Proof see in appendix

In practice, the inner loop cannot guarantee instantaneous perfect tracking of the of the desired acceleration, therefore by considering the error $\hat{\ddot{\boldsymbol{\xi}}} = \ddot{\boldsymbol{\xi}}_r - \ddot{\boldsymbol{\xi}}$, the outer loop error dynamics becomes

$$\dot{\boldsymbol{v}}_{\boldsymbol{e,d}} - \dot{\boldsymbol{v}}_{\boldsymbol{e}} = -\boldsymbol{K}_v(\boldsymbol{v}_{\boldsymbol{e,d}} - \boldsymbol{v}_{\boldsymbol{e}}) - \boldsymbol{K}_p \boldsymbol{e} + \boldsymbol{J}_\xi \hat{\ddot{\boldsymbol{\xi}}}, \quad (36)$$

The perturbation term $J_\zeta \dddot{\tilde{\zeta}}$ can be upper bounded as The norm $||\boldsymbol{J}_\xi||$ is bounded since all the manipulator joints are revolute joints, therefore the first term can be viewed as a vanishing perturbation.

$$||J_\zeta \dddot{\tilde{\zeta}}|| \leq ||J_\zeta|| ||\ddot{\tilde{\zeta}}|| \leq ||J_\zeta|| ||\dot{z}_2|| \leq ||J_\zeta|| (||\Omega|| ||z|| + ||\widetilde{\delta}||)$$

$$\leq ||J_\zeta|| ||\omega|| ||\widetilde{z}|| + ||J_\zeta|| ||\Lambda|| ||\widetilde{\chi}||.$$

In the case $\boldsymbol{\varsigma} = \boldsymbol{0}$ the second term in the above equation is, at least, bounded, since, from Theorem 1, $\widetilde{\boldsymbol{\chi}}$ is at least bounded, while, as already specified, $\boldsymbol{\Lambda}$ is a norm bounded. Therefore, the convergence properties of the two-loop system, described by (33), (36) , are stated by the following theorem.

If the PE condition cannot be met and/or bounded interpolation error ($||\varsigma|| \leq \overline{\varsigma}$) is present, $J_\zeta \dddot{\tilde{\zeta}}$ can be seen as a bounded non-vanishing perturbation and the errors ϵ and z are only bounded (Lemma 9.2 in Khalil (1996)).

Simulation Results

The dynamic model of the whole system has been developed using Python by considering a quadrotor equipped with a 5-DOF robotic manipulator with all revolute joints. In the simulation model, to set both the dynamic parameters (mass and inertia moments) and the Denavit-Hartenberg parameters for the robotic arm, are selected as follows:

Joint	d[mm]	a[mm]	alpha[rad]	theta[rad]
1	0	0	$-\pi/2$	q1
2	0	150	$\pi/2$	q2
3	0	8	0	q3
4	0	0	$-\pi/2$	q4
5	18	0	0	q5

Gains	Values
$K_{p,P}$	$12I_3$
$K_{P,V}$	$5I_3$
$K_{\psi,P}$	8
$K_{\psi,V}$	3
$K_{\phi,P}$	2
$K_{\phi,V}$	1
β	4
$K_{Q,P}$	$140I_5$
$K_{Q,V}$	$20I_5$
$K_{\theta,P}$	2
$K_{\theta,V}$	1
K_P	$7.5I_6$
K_V	$0.6I_6$

Noises generated are: Joint position noise, Robot position noise, Robot orientation noise, Attitude rate noise. All the measured data have been considered available at a frequency rate of 250 Hz. Moreover, a rotation of $\pi/5$ rad along roll, pitch and yaw axes is required as well. The following are also selected: Drag coefficient $= 7.5 \times 10^{-7}$, thrust coefficient $= 3 \times 10^{-5}$. Compensation of the Centrifugal and Coriolis terms, C, has been neglected. Links masses selected are as follows: Link1- 80g, Link2- 10g, Link3- 6g, Link- 2g, Link5- 1.5g.

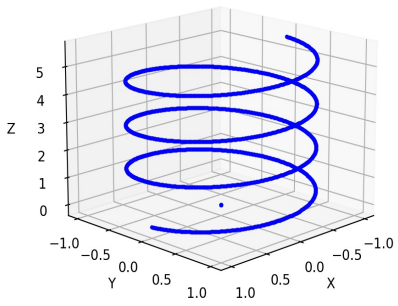

Figure 3: End-Effector Desired trajectory

The Figure 3, reports the end-effector desired trajectory together with the trajectories obtained by using the model-based adaptive law.

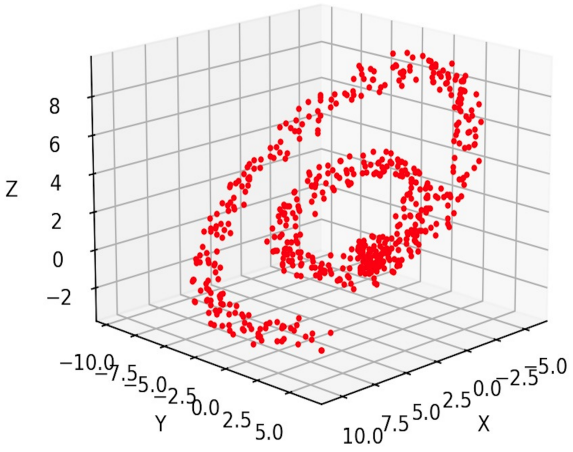

Figure 4: End-Effector obtained trajectory

The Figure 3, reports the end-effector obtained trajectory by using the model-based adaptive law.

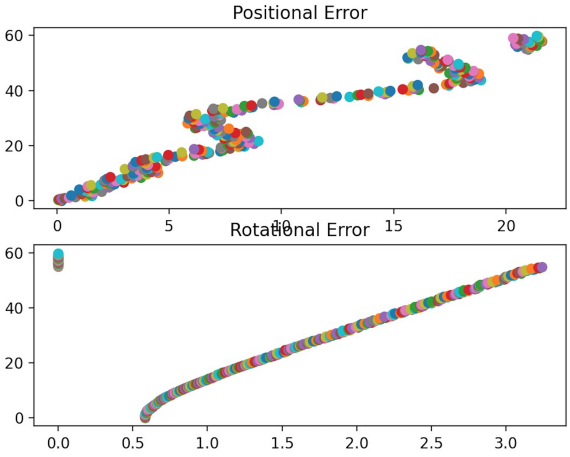

Figure 5: Position and rotation error

The Figure 4, reports the Position and rotation error between the obtained and the desired trajectories

Conclusion

In this paper, a hierarchical motion control scheme has been proposed for an aerial manipulator, composed of a multirotor aerial vehicle equipped with a multi-DOFs robotic arm. First, on the basis of the desired pose of the manipulator end-effector, a closed-loop inverse kinematics algorithm computes the references for the vehicle position, the vehicle yaw angle and the manipulator joints. Then, a cascade controller, with an adaptive term designed to counteract uncertainties, ensures tracking of the desired trajectories. The stability of the proposed control scheme has been theoretically proven. A realistic simulation case study has been developed, in which the algorithm is tested in the presence of digital implementation of the controller, measurement noise and disturbances.

References

1. Doitsidis, L., Weiss, S., Renzaglia, A., Kosmatopoulos, E., Siegwart, R., Scaramuzza, D., Achtelik, M.: Optimal surveillance coverage for teams of micro aerial vehicles in gps-denied environments using onboard vision. Autonomous Robots (2012)
2. Maza, I., Kondak, K., Bernard, M., Ollero, A.: Multi-UAV cooperation and control for load transportation and deployment. Journal of Intelligent and Robotic Systems 57, 417–449 (2010)
3. Maza, I., Ollero, A.: Autonomous transportation and deployment with aerial robots for search and rescue missions. Journal of Field Robotics 28(6), 914931 (2011)
4. Merino, L., Caballero, F., Martinez-de-Dios, J., Maza, I., Ollero, A.: An unmanned aircraft system for automatic forest fire monitoring and measurement. Journal of Intelligent and Robotic Systems 65(1), 533–548 (2012)
5. How, J., Bethke, B., Frank, A., Dale, D., Vian, J.: Real-time indoor autonomous vehicle test environment. IEEE Control Systems Magazine 28(2), 51–64 (2008)
6. Civita, M.L., Papageorgiou, G., Messner, W., Kanade, T.: Design and flight testing of an H_∞ controller for a robotic helicopter. Journal of Guidance, Control, and Dynamics 29(2), 485–494 (2006)
7. Kim, H., Shim, D.: A flight control system for aerial robots: Algorithms and experiments. Control Engineering Practice 11(2), 1389–1400 (2003)
8. Ahanda, J.J.B.M., Mbede, J.B., Melingui, A., Essimbi, B.: Robust adaptive control for robot manipulators: Support vector regression-based command filtered adaptive backstepping approach. Robotica 36(4), 516–534 (2018)
9. Madani, T., Benallegue, A.: Backstepping sliding-mode control applied to a miniature quadrotor flying robot. In: Proc. of the 32nd Annual Conference of the IEEE Industrial Electronics Society, pp. 700–705 (2006)
10. Palunko, I., Fierro, R.: Adaptive control of a quadrotor with dynamic changes in the center of gravity. In: Proc. of the 18th IFAC World Congress, pp. 2626–2631 (2011)
11. Antonelli, G., Cataldi, E., Arrichiello, F., Giordano, P.R., Chiaverini, S., Franchi, A.: Adaptive trajectory tracking for quadrotor mavs in presence of parameter uncertainties and external disturbances. IEEE Transactions on Control Systems Technology 26(1), 248–254 (2018)
12. Kendoul, F., Fantoni, I., Lozano, R.: Asymptotic stability of hierarchical inner-outer loop-based flight controllers. In: Proc. of the 17th IFAC World Congress, pp. 1741–1746 (2008)
13. Pounds, P., Bersak, D., Dollar, A.: Grasping from the air: Hovering capture and load stability. In: Proc. of IEEE Int. Conf. on Robotics and Automation (ICRA), pp. 2491–2498 (2011)
14. Mellinger,D.,Lindsey,Q.,Shomin,M.,Kumar,V.:Design, modelling, estimation and control for aerial grasping and manipulation. In: Proc. of IEEE/RSJ International Conference on Intelligent Robots and Systems, pp. 2668–2673 (2011)
15. Ruggiero, F., Lippiello, V., Ollero, A.: Aerial manipulation: A literature review. IEEE Robotics and Automation Letters 3(3), 1957–1964 (2018)
16. Kondak, K., Krieger, K., Albu Schaeffer, A., Ollero, A.: Closed-loop behavior of an autonomous helicopter equipped with a robotic arm for aerial manipulation tasks. International Journal of Advanced Robotic Systems 10, 1–9 (2013)
17. Huber, F., Kondak, K., Krieger, K., Sommer, D., Schwarzbach, M., Laiacker, M., Kossyk, I., Parusel, S., Haddadin, S., Albu-Schaffer, A.: First analysis and experiments in aerial manipulation using fully actuated redundant robot arm. In: Intelligent Robots and Systems (IROS), 2013 IEEE/RSJ International Conference on, pp. 3452–3457 (2013)
18. Kondak, K., Huber, F., Schwarzbach, M., Laiacker, M., Sommer, D., Bejar, M., Ollero, A.: Aerial manipulation robot composed of an autonomous helicopter and a 7 degrees of freedom industrial manipulator. In: Robotics and Automation (ICRA), 2014 IEEE International Conference on, pp. 2107–2112 (2014)
19. Antonelli, G., Cataldi, E.: Adaptive control of arm-equipped quadrotors. theory and simulations. In: Proceedings of 22th Mediterranean Conference on Control and Automation (2014)
20. Fumagalli, M., Naldi, R., Macchelli, A., Forte, F., Keemink, A., Stramigioli, S., Carloni, R., Marconi, L.: Developing an aerial manipulator prototype: Physical interaction with the environment. IEEE Robotics Automation Magazine 21(3), 41–50 (2014)
21. Kim, S., Choi, S., Kim, H.: Aerial manipulation using a quadrotor with a two dof robotic arm. In: Intelligent Robots and Systems (IROS), 2013 IEEE/RSJ International Conference on, pp. 4990–4995 (2013)
22. Orsag, M., Korpela, C., Oh, P.: Modeling and control of MM-UAV: Mobile manipulating unmanned aerial vehicle. Journal of Intelligent and Robotic Systems 69, 227–240 (2013)
23. Lippiello, V., Ruggiero, F.: Cartesian impedance control of uav with a robotic arm. In: Proc. of 10th International IFAC Symposium on Robot Control (SYROCO), pp. 704–709 (2012)
24. Ryll, M., Muscio, G., Pierri, F., Cataldi, E., Antonelli, G., Caccavale, F., Franchi, A.: 6d physical interaction with a fully actuated aerial robot. In: Robotics and Automation (ICRA), 2017 IEEE International Conference on, pp. 5190–5195. IEEE (2017)
25. Arleo, G., Caccavale, F., Muscio, G., Pierri, F.: Control of quadrotor aerial vehicles equipped with a robotic arm. In: Proc. of 21th Mediterranean Conference on Control and Automation, pp. 1174–1180 (2013)
26. Kannan, S., Bezzaoucha, S., Guzman, S.Q., Dentler, J., Olivares-Mendez, M.A., Voos, H.: Hierarchical control of aerial manipulation vehicle. In: AIP Conference Proceedings, vol. 1798, pp. 1–7. AIP Publishing (2017)
27. Caccavale, F., Giglio, G., Muscio, G., Pierri, F.: Adaptive control for UAVs equipped with a robotic arm. In: Proceedings of the 19th World Congress The International Federation of Automatic Control (IFAC), pp. 11,049–11,054 (2014)
28. Baizid,K., Giglio,G., Pierri,F., Trujillo,M.A., Antonelli, G., Caccavale,F., Viguria,A., Chiaverini,S., Ollero, A.: Behavioral control of unmanned aerial vehicle manipulator systems. Autonomous Robots 41(5), 1203–1220 (2017)

29. Ren, J., Liu, D.X., Li, K., Liu, J., Feng, Y., Lin, X.: Cascade pid controller for quadrotor. 2016 IEEE International Conference on Information and Automation (ICIA) pp. 120–124 (2016)
30. Siciliano, B., Sciavicco, L., Villani, L., Oriolo, G.: Robotics – Modelling, Planning and Control. Springer, London, UK (2009)
31. Nonami, K., Kendoul, F., Suzuki, S., Wang, W.: Atonomous Flying Robots, Unmanned Aerial Vehicles and Micro Aerial Vehicles. Springer, London, UK (2010)
32. Caccavale, F., Chiaverini, S., Siciliano, B.: Second-order kinematic control of robot manipulators with jacobian damped least-squares inverse: Theory and experiments. IEEE/ASME Transactions on Mechatronics 2, 188–194 (1997)
33. Chiaverini, S., Siciliano, B.: The unit quaternion: A useful tool for inverse kinematics of robot manipulators. Systems Analysis Modelling Simulation 35, 45–60 (1999)
34. Muscio, G., Pierri, F., Trujillo, M., Cataldi, E., Antonelli, G., Caccavale, F., Viguria, A., Chiaverini, S., Ollero, A.: Coordinated control of aerial robotic manipulators: Theory and experiments. IEEE Transactions on Control Systems Technology (2017)
35. Hsu, P., Hauser, J., Sastry, S.: Dynamic control of redundant manipulators. In: Proc. of IEEE International Conference on Robotics and Automation (ICRA), pp. 183–187 vol.1 (1988)
36. Reger, J., Ram ırez, H.S., Fliess, M.: On non-asymptotic observation of nonlinear systems. In: Proceedings of the 44th IEEE Conference on Decision and Control, pp. 4219–4224. IEEE (2005)
37. Caccavale, F., Marino, A., Muscio, G., Pierri, F.: Discrete-time framework for fault diagnosis in robotic manipulators. IEEE Transactions on Control Systems Technology 21(5), 1858–1873 (2013)
38. Park, J., Sandberg, I.: Universal approximation using radial-basis-function networks. Neural Computation 3, 246–257 (1991)
39. Khalil, H.: Nonlinear Systems (2nd ed.). Prentice Hall, Upper Saddle River, NJ (1996)
40. Astrom, K., Wittenmark, B.: Adaptive control (2nd ed.). Addison-Wesley (1995)
41. Ioannou, P., Sun, J.: Robust Adpative Control. Prentice Hall, Upper Saddle River, NJ (1996)
42. Wang, C., Hill, D.J.: Learning from neural control. Neural Networks, IEEE Transactions on 17(1), 130–146 (2006)
43. Tayebi, A., McGilvray, S.: Attitude stabilization of a vtol quadrotor aircraft. Control Systems Technology, IEEE Transactions on 14(3), 562–571 (2006)
44. Cano, R.,P'erez, C., Pruano, F., Ollero, A., Heredia, G.: Mechanical design of a 6-DOF aerial manipulator for assembling bar structures using UAVs. In: 2nd RED-UAS 2013 Workshop on Research, Education and Development of Unmanned Aerial Systems (2013)
45. ARCAS - Aerial Robotics Cooperative Assembly System. URL http://www.arcas-project.eu
46. Castaldi, P., Mimmo, N., Naldi, R., Marconi, L.: Robust trajectory tracking for underactuated vtol aerial vehicles: Extended for adaptive disturbance compensation. In: Proc. of 19–th IFAC World Congress, vol. 19, pp. 3184–3189 (2014)
47. Sontag, E.: A remark on the converging-input converging-state property. Automatic Control, IEEE Transactions on 48(2), 313–314 (2003)

Appendix

Proofs

Proof of Corollary 1

In order to prove the Corollary 1, by considering the state space equation of the system (33), with the parameters' estimation error having the following dynamics

$$\dot{\tilde{\boldsymbol{\chi}}} = -\dot{\hat{\boldsymbol{\chi}}} = -\frac{1}{\beta}\boldsymbol{\Lambda}^{\boldsymbol{T}}\boldsymbol{B}^{\boldsymbol{T}}\boldsymbol{Q}\begin{bmatrix}\tilde{\boldsymbol{\xi}}\\ \dot{\tilde{\boldsymbol{\xi}}}\end{bmatrix}$$

and the augmented state $\bar{\boldsymbol{z}}^T = [\tilde{\boldsymbol{z}}^T \ \tilde{\boldsymbol{\chi}}^T]^T$, the close-loop dynamics of the inner loop can be rewritten as the following time-varying system

$$\begin{Bmatrix}\dot{\bar{\boldsymbol{z}}} = \boldsymbol{A}(t)\bar{\boldsymbol{z}}\\ \boldsymbol{y} = \boldsymbol{L}\bar{\boldsymbol{z}}\end{Bmatrix},$$

with

$$\boldsymbol{A}(t) = \begin{bmatrix}\boldsymbol{\Omega} & \boldsymbol{B}\boldsymbol{\Lambda}\\ -\frac{1}{\beta}\boldsymbol{\Lambda}^{\boldsymbol{T}}\boldsymbol{B}^{\boldsymbol{T}}\boldsymbol{Q} & \boldsymbol{O}_p\end{bmatrix},$$

and

$$\boldsymbol{L} = \begin{bmatrix}\sqrt{\boldsymbol{p}_z} & \boldsymbol{O}\\ \boldsymbol{O} & \boldsymbol{O}\end{bmatrix},$$

where $\boldsymbol{p}_z$ is the solution to the Lyapunov equation. The Lyapunov function can be bounded as follows:

$$\frac{1}{2}min\{\lambda_m(\boldsymbol{Q}),\beta\}||\bar{\boldsymbol{z}}||^2 \leq V_i \leq \lambda_m(\boldsymbol{Q}),\beta\}||\bar{\boldsymbol{z}}||^2$$

while the time derivative

$$\dot{V}_i \leq -\bar{\boldsymbol{z}}^T\boldsymbol{L}^T\boldsymbol{L}\bar{\boldsymbol{z}}$$

to prove the exponential stability, it is sufficient to show that the condition

$$\int_t^{t+\delta t}\dot{V}_i(\sigma)d\sigma \leq -\lambda\dot{V}_i(t), \lambda > 0,$$

is met. To this aim, it is worth considering the evolution of V_i on the time interval $[t,\ t+\delta t]$ for some $\delta t > 0$

$$\int_t^{t+\delta t}\dot{V}_i(\sigma)d\sigma = -\int_t^{t+\delta t} -\bar{\boldsymbol{z}}^T\boldsymbol{L}^T\boldsymbol{L}\bar{\boldsymbol{z}}d\sigma = -\bar{\boldsymbol{z}}^T\boldsymbol{W}(t,\ t+\delta t)\bar{\boldsymbol{z}}$$

where $\boldsymbol{W}(t,\ t+\delta t)$ is the observability Gramian of the pair $(\boldsymbol{A},\boldsymbol{L})$. The pair $(\boldsymbol{A},\boldsymbol{L})$ is uniformly observable, i.e. $\boldsymbol{W}(t,\ t+\delta t) \leq k_w\boldsymbol{I}$ $(k_w > 0)$, if and only if the pair $(\boldsymbol{A}-\boldsymbol{K}\boldsymbol{L},\boldsymbol{L})$ is uniformly observable, where $\boldsymbol{K}$ can be chosen, the observability of the pair $(\boldsymbol{A}-\boldsymbol{K}\boldsymbol{L},\boldsymbol{L})$ is proven and, thus, the following condition holds:

$$\int_t^{t+\delta t}\dot{V}_i(\tilde{z}(\sigma))d\sigma \leq -\frac{2k_w}{max\{\lambda_m(\boldsymbol{Q}),\beta\}}V_i(\tilde{\boldsymbol{z}},\tilde{\boldsymbol{\chi}})$$

In conclusion, both $\tilde{\boldsymbol{z}}$ and $\tilde{\boldsymbol{\chi}}$ are exponentially convergent to zero.

Proof of Theorem 3

In order to prove Theorem 3, it is worth defining the following Lyapunov function

$$V = V_o(\epsilon) + \bar{V}_i(\tilde{\boldsymbol{z}},\tilde{\boldsymbol{\chi}}),$$

where $\bar{V}_i$ is a Lyapunov function satisfying the following conditions

$$c_1||\bar{\boldsymbol{z}}||^2 \leq V_i(\bar{\boldsymbol{z}}) \leq c_2||\bar{\boldsymbol{z}}||^2,$$
$$\dot{\bar{V}}_i \leq -c_3||\bar{\boldsymbol{z}}||^2,$$
$$\left|\left|\frac{\partial \bar{V}_i}{\partial \bar{\boldsymbol{z}}}\right|\right| \leq c_4||\bar{\boldsymbol{z}}||,$$

or some positive constants c_1, c_2, c_3 and c_4 and $\bar{\boldsymbol{z}}^T = [\tilde{\boldsymbol{z}}^T \ \tilde{\boldsymbol{\chi}}^T]^T$. Since the conditions of Corollary 1 are satisfied, the exponential stability of the inner loop ensures the existence of such $\bar{V}_i$.